Int J Thermophys (2007) 28:1074–1084
DOI 10.1007/s10765-007-0232-9

Thermophysical Properties of Rare-Earth-Stabilized Zirconia and Zirconate Pyrochlores as Surrogates for Actinide-Doped Zirconia

Keiichi Shimamura · Tatsumi Arima · Kazuya Idemitsu · Yaohiro Inagaki

Published online: 3 August 2007

Abstract Thermophysical properties of rare-earth-stabilized zirconia and zirconate pyrochlores, $A_2Zr_2O_7$ (A = La, Nd, Sm, Gd, Dy, Y), were evaluated by X-ray diffractometry, Raman spectroscopy, and the ultrasound pulse-echo method. Crystallographic analyses elucidated that $La_2Zr_2O_7$, $Nd_2Zr_2O_7$, $Sm_2Zr_2O_7$, and $Gd_2Zr_2O_7$ had the pyrochlore structure, whereas $Dy_2Zr_2O_7$ and $Y_2Zr_2O_7$ had the defect fluorite structure. For lanthanide pyrochlores, the thermal expansion became smaller with increasing ionic radius of A and increasing crystal binding energy. The elastic moduli and Debye temperature evaluated using longitudinal and transverse sound velocities also depend on the ionic radius and binding energy, and hence these values related to mechanical properties increase with the ionic radius of A. On the other hand, Poisson's ratio was almost comparable among these pyrochlores. In addition, thermophysical properties of actinide pyrochlore are discussed in this study.

Keywords Defect fluorite zirconia · Elastic modulus · Sound velocity · Thermal expansion · Zirconate pyrochlore

1 Introduction

Plutonium (Pu) and minor actinides (MA) such as Np, Am, and Cm are generated through reprocessing of spent fuel from light water reactors (LWR). Moreover, the stockpile of weapon-grade Pu from dismantled weapons is increasing in nuclear nations. Pu has already been used in UO_2–PuO_2 solid solutions in LWRs and will be used in fast reactors. However, considering nuclear nonproliferation, an innovative

K. Shimamura (✉) · T. Arima · K. Idemitsu · Y. Inagaki
Department of Applied Quantum Physics and Nuclear Engineering, Faculty of Engineering, Kyushu University, 744 Motooka, Fukuoka 819-0395, Japan
e-mail: keiichi1@nucl.kyushu-u.ac.jp

nuclear fuel system should be developed in order to burn out Pu more efficiently and not to reprocess it. On the other hand, it is possible for MA, which have a long half-life and radiotoxicity, to be disposed in a deep stratum in the form of high-level radioactive waste following transformation into short half-life nuclides or non-radioactive nuclides in nuclear reactors or accelerators.

For these reasons, inert matrix fuels (IMFs) have been developed in the last decade [1]. Inert matrix fuels involve fuel elements, e.g., Pu or MA, that are embedded in the matrices that are inactive against neutrons. Up to now, we have studied the zirconia-based inert matrix fuel, i.e., $Er_xY_yPu_zZr_{1-x-y-z}O_{2-(x+y)/2}$, from theoretical and experimental points of view [2,3]. Such zirconia-based IMFs are stable in a radioactive environment and also have chemical stability [4]. In addition, they are expected to burn out Pu effectively. In this study, we, therefore, focused on the zirconate pyrochlore that is similar to stabilized-zirconia in physicochemical properties.

Zirconate pyrochlore oxides having the chemical formula $A_2Zr_2O_7$ are also candidates for IMFs, where A is Pu or MA. The pyrochlore structure can be considered as an ordered defect fluorite and differs from the fluorite structure in the following ways [5,6]. First, the pyrochlore structure has a different formula than the fluorite structure $(A,Zr)_4O_8$. Second, there is a regular alternation of A and Zr ions in the cation sub-lattice sites of the fluorite. This zirconate pyrochlore IMF has the following advantages: (a) high stability under irradiation; (b) extremely low rate of neutron absorption of zirconium; and (c) chemical and geological stability. So the spent IMF can be disposed directly without reprocessing. Although its thermal conductivity is low, it can be used as fuel by mixing with ceramics or metal, both of which have higher thermal conductivity [7].

So far, the thermochemical properties of the zirconate pyrochlores have been investigated in the nuclear waste form of this material and as an inert matrix fuel [8,9]. For the safety of fuel management, it is also necessary to know the thermophysical properties such as thermal expansion, elastic moduli, Debye temperature, etc. In this study, these properties were evaluated for the system $A_2Zr_2O_7$ using rare-earth metals (A = La, Nd, Sm, Gd, Dy, Y) as surrogates for actinides. For evaluation of elastic moduli, we employed the ultrasound pulse-echo method.

2 Experimental Procedures

2.1 Sample Preparation

The oxide samples $A_2Zr_2O_7$ (A = La, Nd, Sm, Gd, Dy, Y) were synthesized through a solid-state reaction using commercially purchased powder of ZrO_2, La_2O_3, Nd_2O_3, Sm_2O_3, Gd_2O_3, Dy_2O_3, and Y_2O_3 as starting materials. The weighted zirconia and rare earth oxide powders were mixed with ethanol as the dispersant in a mortar. After drying, the powder mixtures were molded by the uniaxial stress. Subsequently, the molded samples were further pressed by the cold isotropic pressure(CIP) method. The compacts thus obtained were sintered at 1,400–1,600°C for 8 h in air. This conventional synthesis process is called the powder-sintering method. The relative density of the

sintered specimens, which were about 10 mm in diameter and 5–10 mm in height, was estimated from the geometrical dimensions and mass.

In addition, a sol-gel method was performed to synthesize powders having high sinterability for the system of $A_2Zr_2O_7$ (A = La, Nd, Sm) [10]. First, the weighted zirconium oxynitrate ($ZrO(NO_3)_2{\cdot}2H_2O$) was added to the solution in which rare earth nitrate ($A(NO_3)_3{\cdot}6H_2O$, A = La, Nd, Sm) was dissolved. Subsequently, citric acid was added to this resultant solution such that the mole ratio of citric acid/zirconium/lanthanum, neodymium, or samarium as the case may be, is 2:1:1. The pH of the resultant metal citrate solution was adjusted to 6–7 by adding dilute ammonia solution drop-wise. Then the solution was slowly evaporated on a water bath until a viscous liquid was obtained. At this stage, the gelating reagent, viz., ethylene glycol, was added such that the mole ratio of citric acid to ethylene glycol was 1:1.2. This mixture was heated on a hot plate/magnetic stirrer at 180°C for about 1 h with constant stirring. When the solution started solidifying and forming a gel like a porous mass, the temperature was increased to 270–280°C until a solid mass was obtained. This solid mass was ground in an agate mortar and then heated at 300–320°C for 30 min. This obtained solid was heated to 400°C to remove the citrates and ethylene glycol. An ash colored substance was obtained at this stage. All these steps were carried out in a draft. This ash colored fine powder was heated at 900°C for 5 h. This product was pressed and sintered as in the case of the powder-sintering method.

2.2 Measurements

X-ray diffraction diffractometry (XRD) with CuKα radiation and Raman spectroscopy using an argon ion laser were employed to characterize the lattice structure for the $A_2Zr_2O_7$ system. Both the measurements were performed at room temperature. In addition, high-temperature XRD (HTXRD) was performed to measure the thermal expansion of $A_2Zr_2O_7$ in the temperature range from 25 to 1, 300°C. In this study, the thermal expansion was obtained as the expansion of the lattice parameter as a function of temperature.

Ultrasound pulse-echo measurements were carried out to estimate the elastic moduli of the samples. The sample was bonded to the transmitting and receiving probe through a coupling agent. The sound velocity in the sample is calculated from the sample length and time separation between ultrasound echoes. The elastic moduli (G: shear modulus, K: bulk modulus, E: Young's modulus, and ν: Poisson's ratio) and Debye temperature (θ_D) were estimated from the ultrasound velocities, i.e., longitudinal (v_l) and transverse (v_s) sound velocities, as follows [11]:

$$G = \rho v_s^2, \tag{1}$$

$$K = \rho v_l^2 - \frac{4}{3}\rho v_s^2, \tag{2}$$

$$E = \frac{9KG}{3K + G}, \tag{3}$$

$$\nu = \frac{E}{2G} - 1, \tag{4}$$

$$\theta_D = \frac{h}{k_B}\left[\frac{9N}{4\pi V(1/v_l^3 + 2/v_s^3)}\right]^{\frac{1}{3}}, \tag{5}$$

where ρ is the density, h is Planck's constant, k_B is the Boltzmann constant, N is the number of atoms in a unit cell, and V is the unit cell volume.

3 Results and Discussions

3.1 Lattice Structure of $A_2Zr_2O_7$

The results of XRD and Raman spectroscopy showed that $La_2Zr_2O_7$, $Nd_2Zr_2O_7$, $Sm_2Zr_2O_7$, and $Gd_2Zr_2O_7$ had the pyrochlore structure, whereas $Dy_2Zr_2O_7$ and $Y_2Zr_2O_7$ had the defect fluorite structure. Figure 1 shows the X-ray diffraction patterns of $A_2Zr_2O_7$ at room temperature. There are found two diffraction peaks such as (331) at around 36° and (511) at around 43° which originate from the pyrochlore structure for the cases of $La_2Zr_2O_7$, $Nd_2Zr_2O_7$, $Sm_2Zr_2O_7$, and $Gd_2Zr_2O_7$. The other peaks are commonly observed for the pyrochlore and defect fluorite structures. No peaks of raw materials such as A_2O_3 or ZrO_2 are observed in these patterns. Figure 2 shows the Raman spectra of $A_2Zr_2O_7$. Raman spectra measurements and XRD measurements are complementary methods to determine whether $A_2Zr_2O_7$ has the pyrochlore structure or the defect fluorite structure. From Fig. 2, it is obvious that the peaks of $La_2Zr_2O_7$, $Nd_2Zr_2O_7$, $Sm_2Zr_2O_7$, and $Gd_2Zr_2O_7$ at particular wave numbers are sharpened, compared with those of $Dy_2Zr_2O_7$ and $Y_2Zr_2O_7$. From the results of the XRD and Raman spectra it was determined that $La_2Zr_2O_7$, $Nd_2Zr_2O_7$, $Sm_2Zr_2O_7$, and $Gd_2Zr_2O_7$ had the pyrochlore structure, and that $Dy_2Zr_2O_7$ and $Y_2Zr_2O_7$ had the defect fluorite structure [12–15].

Figure 3 shows the relationship between the lattice parameter of $A_2Zr_2O_7$ and the ionic radius of A reported by Shannon [16]. Here, the double lattice parameters of $Dy_2Zr_2O_7$ and $Y_2Zr_2O_7$ were plotted to compare with those of $La_2Zr_2O_7$, $Nd_2Zr_2O_7$, $Sm_2Zr_2O_7$, and $Gd_2Zr_2O_7$. This figure clearly shows that the lattice parameter increases linearly with the ionic radius of A [13]. In fact, such an increase in the lattice parameter can be observed for the peak shift toward a lower scattering angle in the X-ray diffraction pattern, as shown in Fig. 1. Related to the crystallographic similarity between lanthanide and actinide pyrochlores, Haire et al. [17] reported that the lattice parameters of actinide pyrochlores increased with the ionic radius of A the same as for lanthanide pyrochlores, which indicates that the lanthanide pyrochlore is a good surrogate for the actinide pyrochlore.

3.2 Thermal Expansion

Figure 4 shows the thermal expansions of $A_2Zr_2O_7$ measured by HTXRD. The thermal expansion was calculated as follows:

$$\alpha = \frac{a_T - a_{298}}{a_{298}}, \tag{6}$$

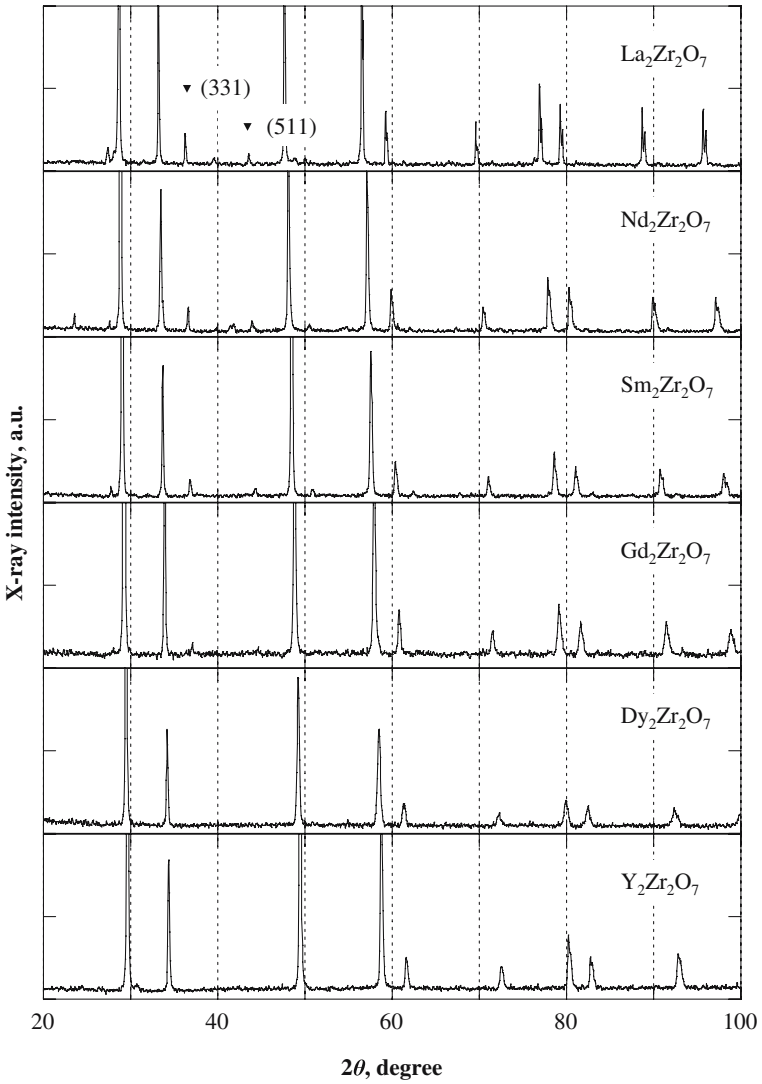

Fig. 1 X-ray diffraction patterns of $A_2Zr_2O_7$. Two peaks indexed (331) and (511) shown for $La_2Zr_2O_7$ originate from the pyrochlore structure, and are also observed for $Nd_2Zr_2O_7$, $Sm_2Zr_2O_7$, and $Gd_2Zr_2O_7$. Other peaks are commonly observed for pyrochlore and fluorite structures

where a_T is the lattice parameter at temperature T [K]. The thermal expansion of zirconate pyrochlores decreased in the order, $Gd_2Zr_2O_7$, $Sm_2Zr_2O_7$, $Nd_2Zr_2O_7$, and $La_2Zr_2O_7$, with an increase in the ionic radius of A. A similar tendency was also reported in Ref. [18]. It indicates that the thermal expansion of zirconate pyrochlores depends on the Madelung binding energy, that is, the larger the Madelung binding energy becomes, the smaller the thermal expansion becomes. According to Subramanian et al. [19], the Madelung binding energy of zirconate pyrochlores depends on

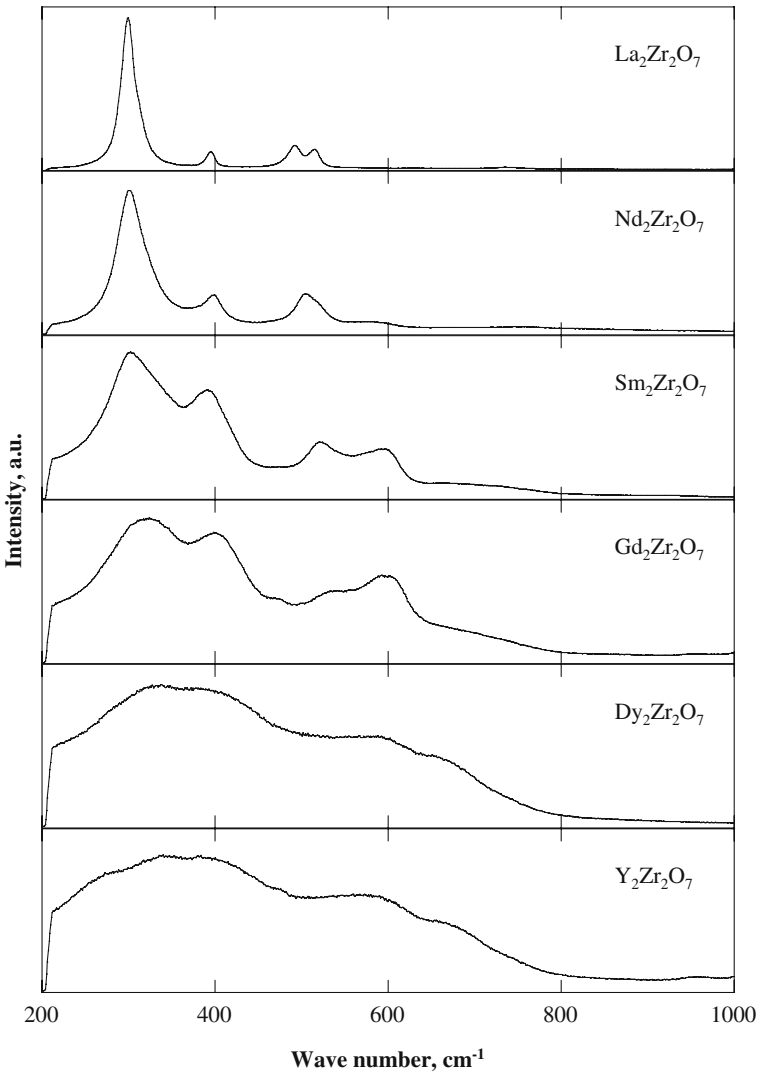

Fig. 2 Raman spectra of $A_2Zr_2O_7$

its oxygen parameter x, and the smaller the value of the oxygen parameter x is, the larger the Madelung binding energy is. The oxygen sub-lattice of pyrochlore consists of O′(8b) and O(48f). And their atomic coordinates are (3/8,3/8,3/8) and (x,1/8,1/8), respectively. They also reported that the larger the ionic radius of A is, the smaller the value of x is. From the standpoint of this idea, the thermal expansion of zirconate pyrochlores should decrease in the order, $Gd_2Zr_2O_7$, $Sm_2Zr_2O_7$, $Nd_2Zr_2O_7$, and $La_2Zr_2O_7$, and the experimental results of this study were in good agreement with the above trend [18,19]. In the same way, the binding energy of defect fluorite might

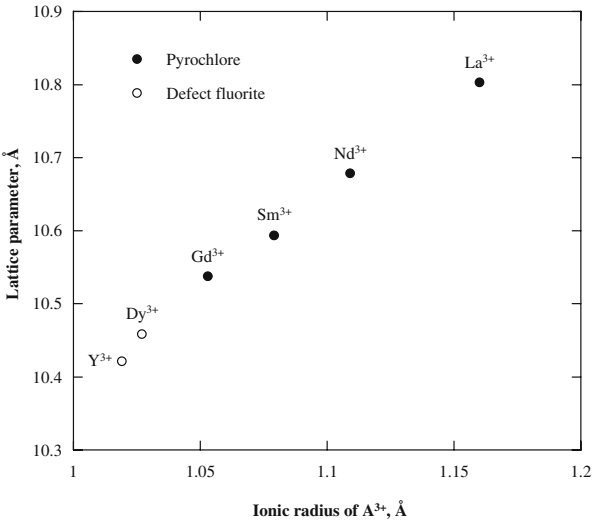

Fig. 3 Lattice parameters of $A_2Zr_2O_7$ as a function of ionic radius of A. Solid and open symbols stand for pyrochlore and defect fluorite structures, respectively

increase in the order, $Dy_2Zr_2O_7$ and $Y_2Zr_2O_7$, because its thermal expansion decreases in the order, $Dy_2Zr_2O_7$ and $Y_2Zr_2O_7$.

3.3 Sound Velocities and Elastic Moduli

Figure 5 shows the relationship between the relative density and the longitudinal or transverse sound velocity of $A_2Zr_2O_7$. The sound velocities of all samples increased linearly with relative densities. Although almost densities of samples fabricated in this study lie under 90%, the elastic moduli and other properties discussed later are calculated using sound velocities extrapolated for a relative density of 100%. In addition, it shows that the value of the sound velocities of zirconate pyrochlores increased in the order, $Gd_2Zr_2O_7$, $Sm_2Zr_2O_7$, $Nd_2Zr_2O_7$, and $La_2Zr_2O_7$, with an increase in the ionic radius of A and hence, an increase in the Madelung binding energy of zirconate pyrochlores as discussed above. It is obvious that the propagation of sound waves is similar to that for micro-strains in the material, and hence that of micro-displacement of atoms that make up the material. So it is reasonable that the sound velocities of materials are related to the binding energy which joins the atoms to each other in the materials. According to this idea, the larger the binding energy of $A_2Zr_2O_7$ becomes, the larger the sound velocities of $A_2Zr_2O_7$ become. As a result, the atomic dependence of the sound velocity shown in Fig. 5 agreed with that of the thermal expansion.

Figure 6 shows the shear, bulk, and Young's moduli calculated from Eqs. (1)–(3). On the other hand, Fig. 7 shows Poisson's ratio and the Debye temperature calculated from Eqs. (4) and (5). Each elastic modulus, which is related directly to the binding energy, is defined as a proportional constant between stress and strain. So the larger the elastic modulus is, the more difficult deformation becomes and hence the higher

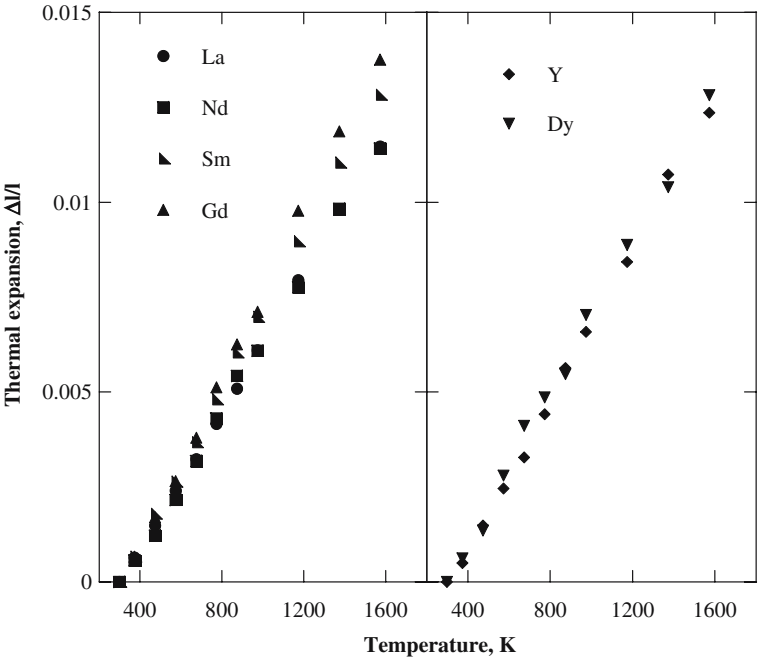

Fig. 4 Thermal expansion of $A_2Zr_2O_7$ as a function of temperature

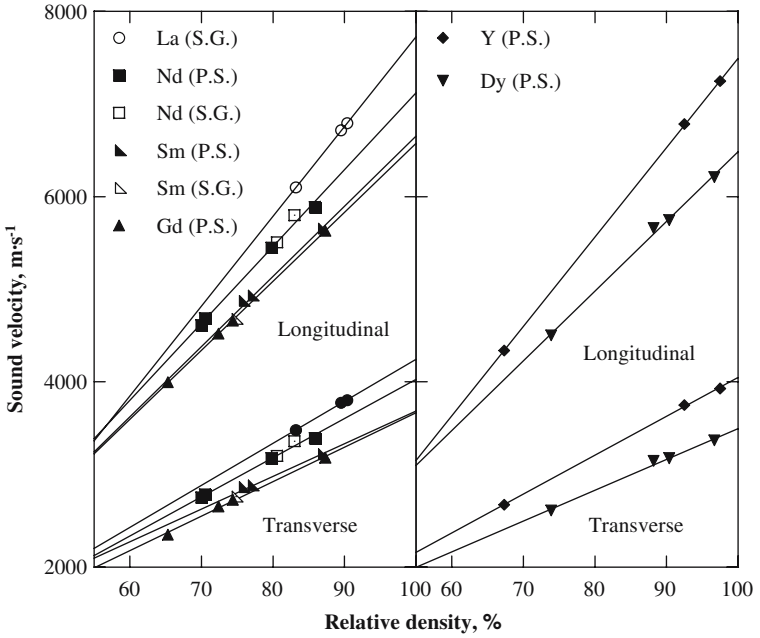

Fig. 5 Longitudinal and transverse sound velocities of $A_2Zr_2O_7$ as a function of relative density. Solid/S.G. and open/P.S. symbols stand for sol-gel and powder-sintering syntheses, respectively

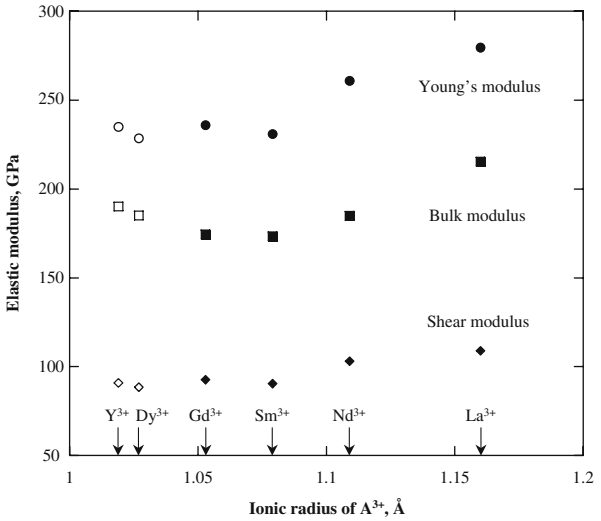

Fig. 6 Elastic moduli of $A_2Zr_2O_7$ as a function of ionic radius of A. Solid and open symbols stand for pyrochlore and defect fluorite structures, respectively

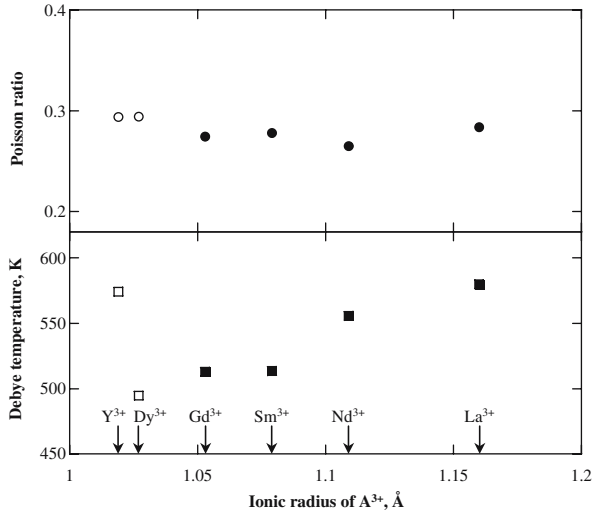

Fig. 7 Poisson's ratio and Debye temperature of $A_2Zr_2O_7$ as a function of ionic radius of A. Solid and open symbols stand for pyrochlore and defect fluorite structures, respectively

the binding energy is. This idea explains the result shown in Fig. 6. On the other hand, Poisson's ratio is not related to the binding energy because it is defined as the ratio of the strain in the radial direction to that in the length direction. Hence, there is no atomic dependence of the experimental result for Poisson's ratio. For the case of the Debye temperature which is related to the material hardness, there is found the atomic dependence as for the elastic moduli.

The present experimental results show that the elastic moduli and other properties discussed here strongly depend on the atomic radius of A (rare-earth metals including lanthanides) for the zirconate pyrochlore $A_2Zr_2O_7$ as well as for stabilized-zirconia. Furthermore, Haire et al. [17] and Raison et al. [20] reported that the lattice parameter of the actinide pyrochlore $An_2Zr_2O_7$ (An: actinide) increased with the ionic radius of An, which means that the lanthanide pyrochlore was a good surrogate for the actinide pyrochlore in terms of the crystal structure. Therefore, if the ionic radius of the actinide ion is known from crystallographic analyses or other methods, it is possible to correctly predict the thermomechanical and crystal properties of $An_2Zr_2O_7$.

4 Conclusion

Rare-earth-stabilized zirconia and zirconate pyrochlores having the $A_2Zr_2O_7$ chemical formula were investigated in terms of their thermophysical properties, where $A_2Zr_2O_7$ (A = La, Nd, Sm, Gd, Dy, Y) were used as surrogates for actinide-doped zirconia. By means of XRD and Raman spectroscopy, the pyrochlore structure was observed for $La_2Zr_2O_7$, $Nd_2Zr_2O_7$, $Sm_2Zr_2O_7$, and $Gd_2Zr_2O_7$, whereas the defect fluorite structure was found for $Dy_2Zr_2O_7$ and $Y_2Zr_2O_7$. In the $A_2Zr_2O_7$ system, the ionic radius of A was determined, independent of whether $A_2Zr_2O_7$ had the pyrochlore or defect fluorite structure. HTXRD measurements showed that the smaller the thermal expansion became, the larger the ionic radius of A was, which indicates that if in the system A ion is large, the binding energy becomes larger for $A_2Zr_2O_7$. The measurement of the sound velocities showed that both longitudinal and transverse sound velocities were increasing with an increase in the ionic radius of A for lanthanide pyrochlores. Consequently, this resulted in increases in the magnitudes of the elastic moduli and Debye temperature. On the other hand, Poisson's ratio of $A_2Zr_2O_7$ was almost insensitive to the ionic radius of A.

In this study, it showed that especially for lanthanide pyrochlores, the ionic radius of A and binding energy of the relevant crystal have a significant effect on thermophysical properties. Considering the similarity between lanthanide and actinide ions for the zirconate pyrochlore, a deeper understanding of crystallographic properties helps us to determine the thermophysical properties of actinide pyrochlores.

Acknowledgments The authors would like to thank M. Watanabe for assistance and advice in XRD measurements and K. Hashizume for Raman spectra measurements.

References

1. C. Degueldre, U. Kasemeyer, F. Botta, G. Ledergerber, Mat. Res. Soc. Symp. Proc. **412**, 15 (1995)
2. T. Arima, S. Yamasaki, S. Torikai, K. Idemitsu, Y. Inagaki, C. Degueldre, J. Alloys Compd. **398**, 296 (2005)
3. K. Idemitsu, T. Arima, Y. Inagaki, S. Torikai, M.A. Pouchon, J. Nucl. Mater. **319**, 31 (2003)
4. K. Kuramoto, N. Nitani, T. Yamashita, J. Nucl. Mater. **319**, 180 (2003)
5. W.R. Cook Jr., H. Jaffe, Phys. Rev. **89**, 1297 (1953)
6. E. Aleshin, R. Roy, J. Am. Ceram. Soc. **45**, 18 (1962)
7. T. Yamashita, K. Kuramoto, H. Akie, Y. Nakano, N. Nitani, T. Nakamura, K. Kusagaya, T. Ohmichi, J. Nucl. Sci. Technol. **39**, 865 (2002)

8. S. Lutique, R.J.M. Konings, V.V. Rondinella, J. Somers, T. Wiss, J. Alloys Compd. **352**, 1 (2003)
9. R.C. Ewing, W.J. Weber, J. Lian, J. Appl. Phys. **95**, 5949 (2004)
10. K.K. Rao, T. Banu, M. Vithal, G.Y.S.K. Swamy, K.R. Kumar, Mater. Lett. **54**, 205 (2002)
11. S. Yamanaka, K. Kurosaki, T. Matsuda, M. Uno, J. Nucl. Mater. **294**, 99 (2001)
12. Y. Tabira, R.L. Withers, J.C. Barry, L. Elcoro, J. Solid State Chem. **159**, 121 (2001)
13. H. Yamamura, H. Hishino, K. Kakinuma, K. Nomura, Solid State Ionics **158**, 359 (2003)
14. W.E. Klee, G. Weitz, J. Inorg. Nucl. Chem. **31**, 2367 (1969)
15. M.T. Vandenborre, E. Hussen, H. Brusset, Spectrochim. Acta **37A**, 113 (1981)
16. R.D. Shannon, C.T. Prewitt, Acta. Cryst. **A32**, 751 (1976)
17. R.G. Haire, P.E. Raison, Z. Assefa, J. Nucl. Sci. Technol. Supplement **3**, 616 (2002)
18. K.V.G. Kutty, S. Rajagopalan, C.K. Mathews, Mat. Res. Bull. **29**, 759 (1994)
19. M.A. Subramanian, G. Aravamudan, G.V.S. Rao, Prog. Solid State Chem. **15**, 55 (1983)
20. P.E. Raison, R.G. Haire, Z. Assefa, J. Nucl. Sci. Technol. Supplement **3**, 725 (2002)